Modulatory dynamics mark the transition between anesthetic states of unconsciousness

Elie Adam[a,b,1,2] (iD), Ohyoon Kwon[a,b,1] (iD), Karla A. Montejo[a,b,1] (iD), and Emery N. Brown[a,b,c,2]

Unconsciousness maintained by GABAergic anesthetics, such as propofol and sevoflurane, is characterized by slow-delta oscillations (0.3 to 4 Hz) and alpha oscillations (8 to 14 Hz) that are readily visible in the electroencephalogram. At higher doses, these slow-delta–alpha (SDA) oscillations transition into burst suppression. This is a marker of a state of profound brain inactivation during which isoelectric (flatline) periods alternate with periods of the SDA patterns present at lower doses. While the SDA and burst suppression patterns have been analyzed separately, the transition from one to the other has not. Using state–space methods, we characterize the dynamic evolution of brain activity from SDA to burst suppression and back during unconsciousness maintained with propofol or sevoflurane in volunteer subjects and surgical patients. We uncover two dynamical processes that continuously modulate the SDA oscillations: alpha-wave amplitude and slow-wave frequency modulation. We present an alpha modulation index and a slow modulation index which characterize how these processes track the transition from SDA oscillations to burst suppression and back to SDA oscillations as a function of increasing and decreasing anesthetic doses, respectively. Our biophysical model reveals that these dynamics track the combined evolution of the neurophysiological and metabolic effects of a GABAergic anesthetic on brain circuits. Our characterization of the modulatory dynamics mediated by GABAergic anesthetics offers insights into the mechanisms of these agents and strategies for monitoring and precisely controlling the level of unconsciousness in patients under general anesthesia.

alpha-wave modulation | slow-wave modulation | oscillations | metabolism | burst suppression

Each anesthetic agent has a distinct neurophysiological signature that is readily visible in the electroencephalogram (EEG) and local field potential, and relates directly to the anesthetic's mechanism of action (1, 2). For this reason, anesthetic EEG signatures can be used to monitor the level of unconsciousness in patients receiving general anesthesia for surgery. In adults, unconsciousness maintained by GABAergic anesthetics such as propofol and sevoflurane is primarily characterized by slow-delta oscillations (0.3 to 4 Hz) and alpha oscillations (8 to 14 Hz) (3). If the anesthetic dose is increased sufficiently, these oscillations transform into burst suppression, a state of profound brain inactivation during which quiescent or isoelectric (flatline) periods are interspersed between bursts of activity (1, 4, 5).

Experimental and modeling studies have shown that the slow-delta–alpha oscillatory state (SDA) is primarily a neurophysiological process (6). The alpha oscillations are a highly coherent thalamus–prefrontal cortex rhythm (7), whereas the slow-delta oscillations represent up–down states during which neural spiking activity is strongly down-regulated across large parts of the cortex (8). The presence of SDA oscillations is considered a marker of an adequate level of unconsciousness for surgery (3). Modeling studies and the clinical use of burst suppression suggest that this state is a neurometabolic phenomenon (4, 9). The quiescent periods disrupt the SDA oscillations when diminished levels of ATP make it difficult for neurons to maintain their membrane potentials (4). The presence of burst suppression is a more profound state of unconsciousness that has been associated with postoperative cognitive disorders, particularly in the elderly (10, 11). This is why for anesthetic management of unconsciousness during surgery it is recommended to dose the anesthetics so as to avoid burst suppression (5). On the other hand, the state of burst suppression is often maintained intentionally for several days or more in intensive care unit patients placed in a medical coma to treat refractory status epilepticus or intracranial hypertension (5, 9).

To date, it is known that modulation of the alpha oscillation amplitude by the phase of the slow oscillation can be a marker of anesthetic state (3, 12). Moreover, alpha suppression periods (13) and decreased alpha amplitude (14) may predict the subsequent appearance of burst suppression. It has also been shown that the lengths of the suppression

Significance

During unconsciousness maintained by GABAergic anesthetics (propofol and sevoflurane), the typical electroencephalogram signatures are slow-delta oscillations (0.3 to 4 Hz) and alpha oscillations (8 to 14 Hz) that at higher doses devolve into burst suppression, a marker of profound brain inactivation. The dynamics of the transition between these states of unconsciousness remain uncharacterized. We report alpha-wave-amplitude and slow-wave-frequency modulatory processes that track continuously the transition between these states in humans anesthetized with either propofol or sevoflurane. Our biophysical model attributes these modulatory dynamics to the combined neurophysiological and metabolic effects of these anesthetics on brain circuits. Our findings offer insights into the mechanisms of these agents and strategies for monitoring and precisely controlling unconsciousness in patients under general anesthesia.

[1]E.A., O.K., and K.A.M contributed equally to the work.

[2]To whom correspondence may be addressed. Email: eadam@mit.edu or enb@neurostat.mit.edu.

periods of burst suppression can be characterized as a function of anesthetic dose and level of hypothermia, another process that can produce burst suppression (15). While SDA oscillations and burst suppression are produced by GABAergic anesthetics, the transition from the former to the latter has not been studied.

The important advance we report is the characterization of the transition from SDA to burst suppression and back to SDA as a function, respectively, of increasing and decreasing doses of propofol or sevoflurane in healthy volunteers and surgical patients. We have identified a modulatory process of brain activity that tracks continuously the transition from the SDA oscillations to burst suppression and back to SDA oscillations. We have found that this modulation occurs in parallel for the alpha and slow oscillations. We develop an alpha modulation index (AMI) and a slow modulation index (SMI) and illustrate their application in EEG recordings from four categories of subjects or patients. We also propose a biophysical model that characterizes the modulation process and how it links the neurophysiological process of the SDA dynamics and the neurometabolic process of burst suppression. In addition to deciphering the link between two robust signatures of anesthesia neurophysiology, our work suggests markers for real-time tracking and control of level of unconsciousness in patients receiving general anesthesia.

Results

Experimental Data. To study the relationship between SDA and burst suppression, we analyzed EEG data from four different groups of patients. Each received either propofol or sevoflurane as the primary anesthetic to maintain unconsciousness. All data were recorded under human studies protocols approved by the Massachusetts General Hospital Human Research Committee. These patients were 10 young (ages 18 to 35 y) healthy volunteers who received increasing followed by decreasing doses of propofol through computer-controlled infusions (3); 10 surgical patients (ages 24 to 82 y) administered propofol by manual titration; 10 surgical patients administered propofol by manual titration whose EEG showed diminished or absent alpha waves (ages 50 to 90 y); and 10 surgical patients (ages 53 to 72 y) administered sevoflurane by manual titration. The EEG data were analyzed using standard multitaper spectral analysis methods, bandpass filtering, and state-space methods as described in *Materials and Methods*. The results for all 40 subjects are given in *SI Appendix,* Figs. S1–S40, and statistical summary of our results is given in *SI Appendix,* Fig. S41 *A–D*.

We restricted the analysis of the modulations during the transition from SDA to burst suppression and back to the periods where the alpha and slow oscillations were present. For the volunteer subjects, this period began following loss of consciousness when the alpha oscillations appeared and lasted until the start of emergence when the alpha oscillations transitioned to beta oscillations, in accordance with the findings in ref. 3. For the surgical patients, this period began following induction when the alpha or slow oscillations appeared and lasted until either anesthetic administration ended or the alpha oscillations transitioned into beta oscillations and/or the slow-delta oscillations dissipated, whichever event occurred first. The periods not analyzed at the start and end of a session are marked in gray in these figures.

Transition from Alpha Oscillations to Burst Suppression and Back in a Healthy Volunteer Administered Propofol. As previously reported from this healthy volunteer experiment (3), with changes in the propofol target effect-site concentration
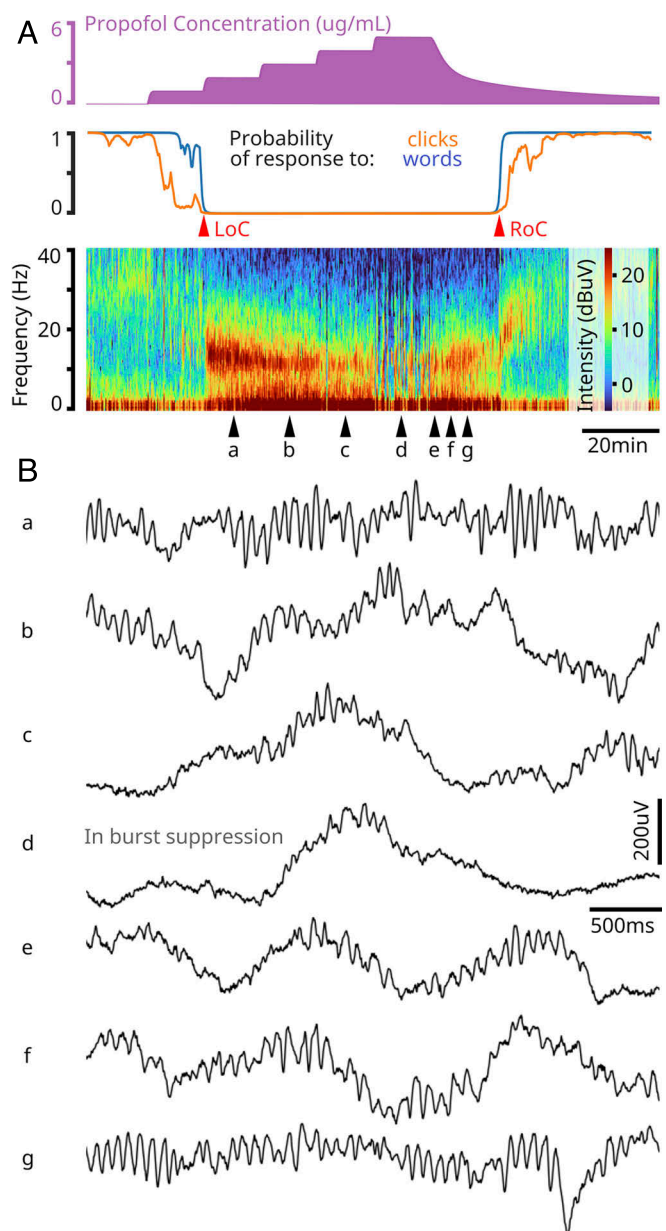

Fig. 1. Evolution of EEG dynamics during propofol-mediated unconsciousness. (*A*) *Top*. Graph shows the target propofol effect-site concentration for a volunteer subject receiving a computer-controlled propofol infusion. The propofol infusion rate is increased in a stepwise manner to achieve 5 increasing target effect-site concentrations then the infusion is turned off. *Middle*. Temporal traces of the correct response probability for verbal cues (blue) and sound clicks (orange) to infer loss (LoC) and recovery (RoC) of consciousness. *Bottom*. EEG Spectrogram. (*B*) Four-second raw EEG segments recorded at the timepoints indicated in (*A*) showing amplitude modulation. The high-frequency variations are predominantly alpha oscillations (8 to 14 Hz), whereas the low-frequency variations are slow-delta oscillations (0.3 to 4 Hz). The *a–g* progression shows the transition during unconsciousness from slow-delta and alpha oscillations into burst suppression (*d*) and back.

(Fig. 1 *A, Upper*), it is possible to track changes in behavioral response (Fig. 1 *A, Middle*) and corresponding changes in the spectral content of the EEG (Fig. 1 *A, Lower*). The first finding we report is a modulation of the alpha oscillation amplitude in which the raw EEG transitions from having high-amplitude alpha oscillations to low-amplitude alpha oscillations. This modulation is present as soon as the alpha oscillations appear shortly after loss of consciousness (Fig. 1 *B, a* and *b*). With increasing propofol target effect-site concentration, the periods of high-amplitude

alpha oscillations decrease, and the periods of low-amplitude alpha oscillations increase (Fig. 1 *B, c*) until the raw EEG signal becomes burst suppression (Fig. 1 *B, d*). As the target propofol effect-site concentration declines (Fig. 1*A*), the periods of low-amplitude alpha oscillations shorten and the periods of high-amplitude alpha oscillations lengthen (Fig. 1 *B, e–g*). Hence, in these young healthy volunteers receiving propofol, the alpha amplitude modulation tracks the transition from the appearance of alpha oscillations to burst suppression and back to alpha oscillations as a function of increasing and decreasing propofol doses.

The alpha amplitude modulation is more apparent when the EEG is filtered to isolate the alpha band (Fig. 2*A*). We further enhanced the presentation of the modulation by defining periods of high-amplitude alpha oscillations as up-states and the periods of low-amplitude alpha oscillations as down-states (Fig. 2 *B* and *C*) (See *Materials and Methods* for a complete definition of the alpha up-states and the alpha down-states). When the data in Fig. 1 are filtered to isolate the alpha band, we see that as the propofol target effect-site concentration increases, the up-state durations decrease and the down-state durations increase

(Fig. 2 *B, a–d*). As the propofol target effect-site concentration decreases, the dynamics reverse (Fig. 2 *B, e* and *f*). As illustrated with the raw EEG signal, burst suppression (Fig. 2 *B, d*) is a point on the alpha amplitude modulation continuum during which alpha down-states are appreciably longer than the up-states. The alpha down-states correspond to the suppression periods.

Our biophysical model, described later, offers an explanation for the changes in these dynamics of the alpha oscillations.

Transition from Slow-Delta Oscillations to Burst Suppression and Back in a Healthy Volunteer Administered Propofol. In addition to alpha-wave modulation, the second finding we report is the presence of a slow-delta oscillation (0.3 to 4 Hz) frequency modulation which is readily visible in the raw EEG recording (Fig. 1*B*) and in the slow-delta band extracted from the raw EEG signal by bandpass filtering (Fig. 2 *A, D,* and *E*). The modulation is apparent when we focus on the duration of the slow cycles and the duration of their down periods (Fig. 2*E*). (See *Materials and Methods* for definitions of the slow cycle and slow down-state durations). At low propofol target effect-site concentrations, isolated large amplitude (up and down) cycles
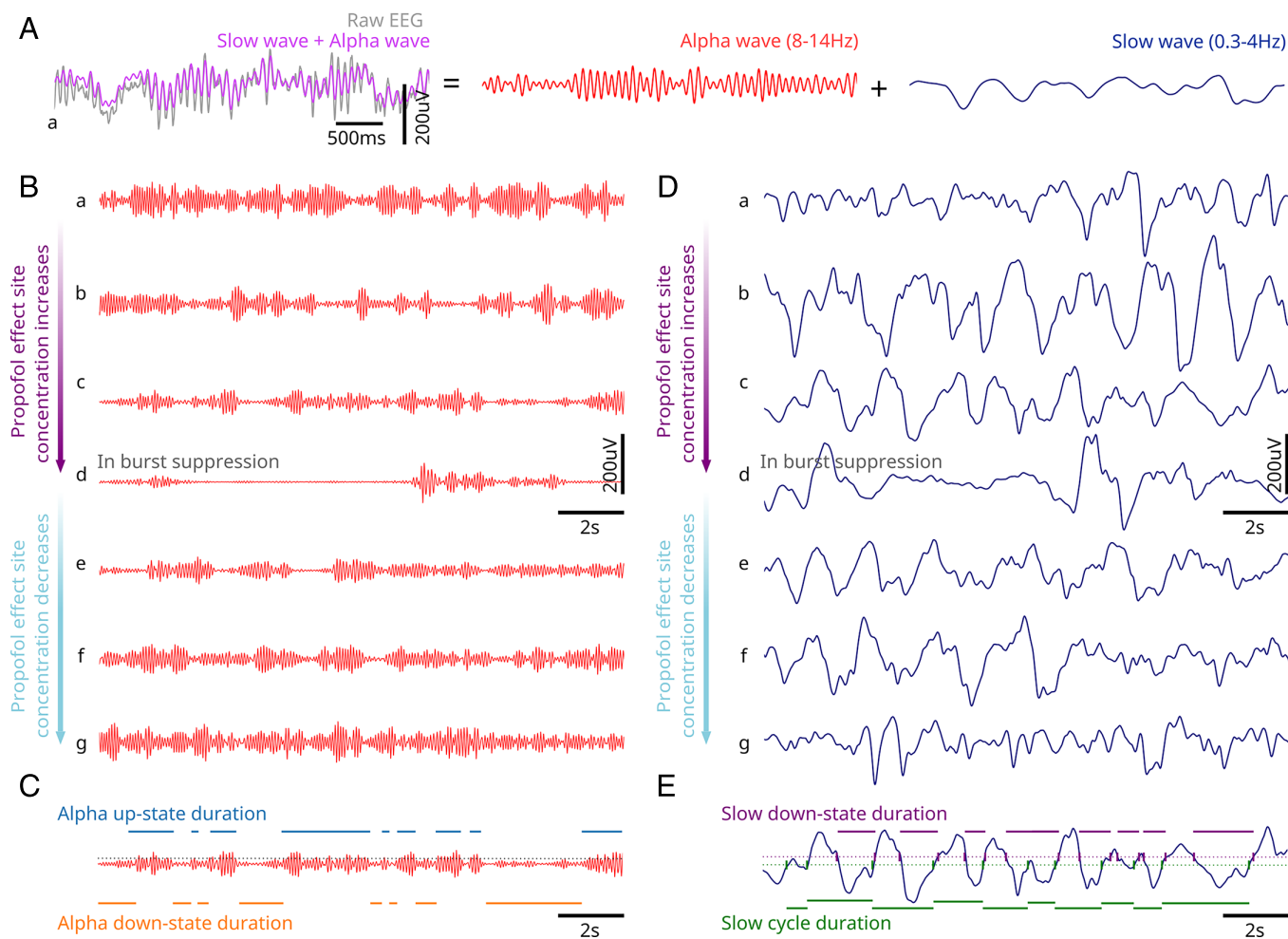

Fig. 2. Alpha- and slow-delta-wave modulation continuously track the transition from SDA to burst suppression and back to SDA during propofol-mediated unconsciousness. (*A*) Raw EEG signal (grey) recorded during propofol-mediated unconsciousness shown along with its alpha oscillation component (red), its slow-delta oscillation component (blue), and the sum of the two (purple). (*B*) EEG traces showing the modulation of the filtered alpha oscillations extracted at the timepoints indicated in Fig. 1 *A* and *B, a–g*. The alpha-wave modulation continuously tracks the transition from SDA to burst suppression and back to SDA during propofol-mediated unconsciousness. The first 4 s correspond to the traces in Fig. 1*B*. (*C*) Trace illustrating alpha-wave up-state durations (blue) and down-state durations (orange) and their computation through thresholding. (*D*) Similar to (*B*) but applied to the filtered slow-delta oscillations. (*E*) Trace illustrating slow-wave cycle durations (green) and down-state durations (purple) and their computation through crossings (green dashed line) and thresholding (purple dashed line), respectively.
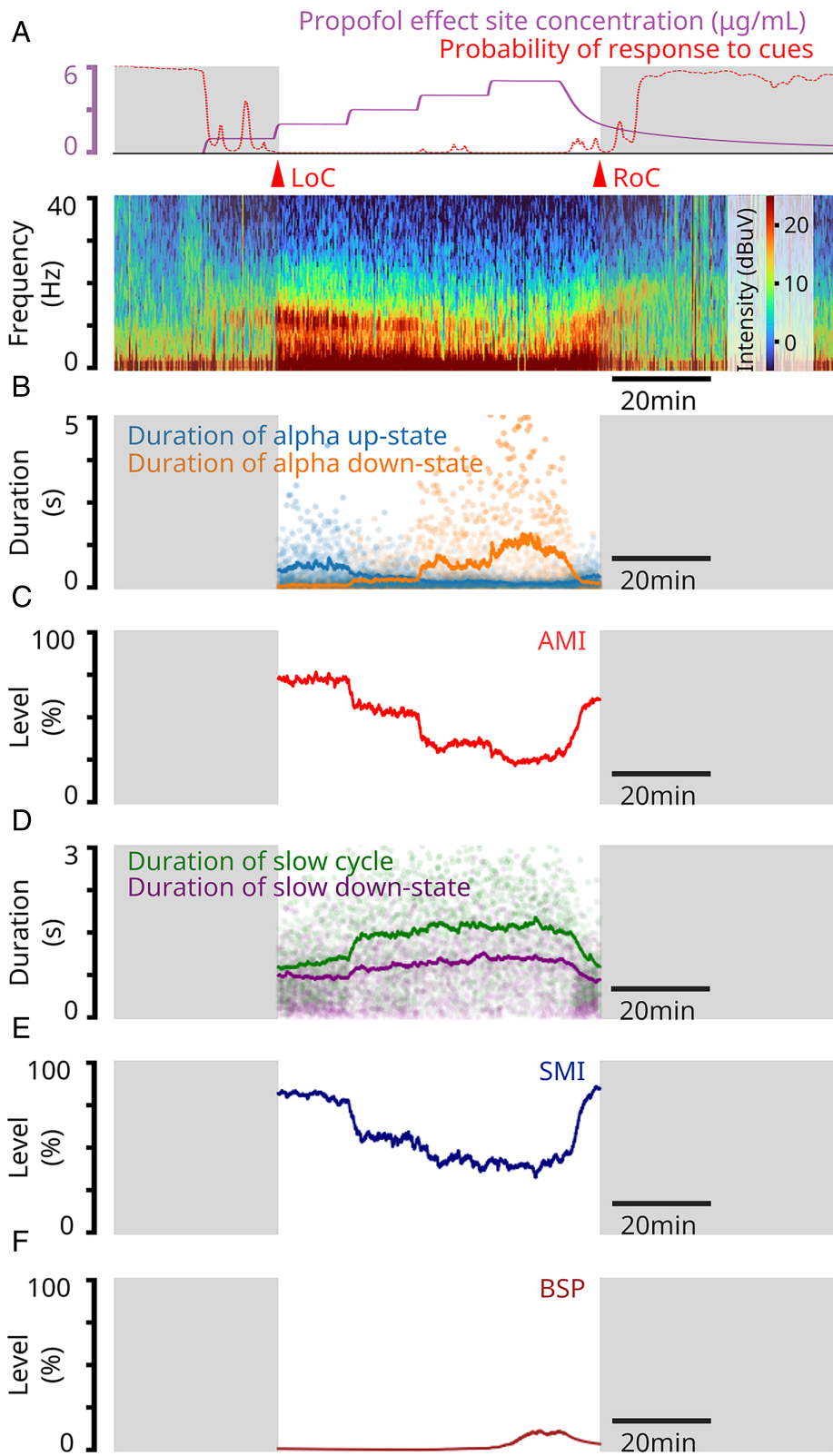
Fig. 3. EEG dynamics of a volunteer subject under propofol-mediated unconsciousness show modulation progression from SDA to burst suppression and back to SDA. (*A*) (*Top*) Propofol target effect-site concentration (purple) and correct response probability curves for cues (red) as in Fig. 1*A*. The red arrows indicate loss (LoC) and recovery (RoC) of consciousness. (*Bottom*) EEG spectrogram. (*B*) Time series plots showing the alpha up-state (blue) and down-state (orange) durations. The smooth traces are Kalman filter estimates of the corresponding mean state durations. (*C*) Time course of the AMI. See *Text* for definition. (*D*) Time series plots showing the slow-oscillation cycle durations (green) and the slow-oscillation down-state durations (purple). The smooth traces are Kalman filter estimates of the corresponding mean state durations. (*E*) Time course of the SMI. See *Text* for definition. (*F*) Time course of the BSP.

begin to appear in the slow waves (Fig. 2*D*). Their durations are distinctly larger than the initial slow-wave fluctuations. These cycles initially appear sparsely in the slow-wave fluctuations. As the propofol target effect-site concentration increases, they occur more frequently (Fig. 2 *D*, *a–d*). The occurrence of these large cycles increases until they coalesce: Their up-states transition to the burst periods of burst suppression, whereas their troughs or down-states transition to the suppression periods of burst suppression (Fig. 2 *D* and *E*). The progression of these dynamics also reverses (Fig. 2 *D*, *e–g*), as the propofol target effect-site concentration decreases.

As with alpha-wave modulation, our biophysical model explains the dynamics of slow-wave modulation.

Alpha- and Slow-Wave Modulation Track Propofol Effect Site Concentration during the Transition from SDA to Burst Suppression and Back. To track quantitatively the EEG dynamics in the alpha band during the transition from SDA to burst suppression and back to SDA, we derived an AMI (*Materials and Methods*). AMI is a real-time measure derived from a ratio between the duration of the alpha up-states and down-states (Fig. 2 *B* and *C*). We tested it on the EEG recordings from all 10 volunteer subjects who underwent propofol-mediated loss and recovery of consciousness. An example is given in Fig. 3. We found that the duration of an alpha up-state decreases as the propofol target effect-site concentration increases, up to a point, after which the duration of an alpha down-state begins to increase (Fig. 3 *A* and *B*). We also found that AMI mirrored the propofol target effect-site concentration (Fig. 3 *A* and *C* and *SI Appendix*, Table S2).

We derived a SMI to track the dynamics of the slow-wave frequency modulation during the transition from SDA to burst suppression and back to SDA (*Materials and Methods*). SMI is a real-time measure derived from a ratio between the frequency of slow-wave cycles and duration of the slow-wave down-state (Fig. 3 *B* and *C*). We found that the number of slow-wave cycles per unit time decreased as the propofol targets effect-site concentration increased, up to a point where the slow-wave down-states became more prominent and began to lengthen (Fig. 3*D*). Like AMI (Fig. 3 *A* and *C*), SMI also mirrored the propofol effect-site concentration (Fig. 3 *A* and *E* and *SI Appendix*, Table S2).

For validation, we computed the burst suppression probability (BSP) which tracks across time the instantaneous probability that a patient is in burst suppression (15) (*Materials and Methods*). We found that both AMI and SMI reflect the information present in BSP which is designed to track high effect-site concentrations (Fig. 3 *C*, *E*, and *F*). That is primarily because the suppressions that the BSP detects coincide with the down-states in the alpha waves and down-states in the slow waves (*Materials and Methods*). More importantly, AMI and SMI track modulatory dynamics that are present at lower propofol target effect-site concentrations. Here, BSP is uninformative (Fig. 3 *C*, *E*, and *F*).

Five of the 10 subjects in our volunteer cohort (cases 1, 3, 6, 7, and 9; see *SI Appendix*, Figs. S1, S3, S6, S7, and S9) undergo a transition from SDA to burst suppression and back to SDA. AMI and SMI tracked these transitions. The remaining five volunteer subjects (cases 2, 4, 5, 8, and 10; see *SI Appendix*, Figs. S2, S4, S5, S8, and S10) stayed in SDA. This demonstrates that AMI and SMI track not only the transitions between SDA and burst suppression but also the dynamics within the SDA stages of propofol-mediated unconsciousness. AMI and SMI track different oscillatory bands and are computed differently

(Fig. 2 *C* and *E*). However, because both indices track the transitions between SDA and burst suppression (*SI Appendix*, Fig. S41*A*), this suggests that the alpha- and slow-wave modulations are likely driven by a common process. Our biophysical model illustrates that this common process is likely due to the combined neurophysiological and metabolic effects of propofol.

Alpha- and Slow-Wave Modulation are Present in Surgical Patients under Propofol-Mediated Unconsciousness. Anesthetic administration to the volunteer subjects used only propofol targeted to achieve specific effect-site concentrations in order to track loss and recovery of consciousness. In surgical cases, the situation is different as multiple agents are administered simultaneously (e.g., hypnotics, analgesics and muscle relaxants) to achieve the state of general anesthesia (16) and not simply unconsciousness (Fig. 4). Nevertheless, the EEG dynamics are governed predominantly by the primary hypnotic agent. We found that the alpha- and slow-wave modulation dynamics are also present in surgical cases during which propofol is the primary hypnotic agent (Fig. 4 *A–E*). In these cases, AMI and SMI tracked the transition from SDA to burst suppression and back (Fig. 4 *B–E*). AMI and SMI track the modulatory dynamics identified by the BSP when burst suppression is present as well as the alpha-wave amplitude and slow-wave frequency modulation present at propofol doses lower than those at which burst suppression occurs (Fig. 4*F*).

Four of the ten patients in our surgical cohort (cases 11, 15, 18, and 20; see *SI Appendix*, Figs. S11, S15, S18, and S20) underwent the transition from SDA to burst suppression and back to SDA during surgery. Both AMI and SMI tracked these transitions. The other six patients (cases 12–14, 16, 17, and 19; see *SI Appendix*, Figs. S12–S14, S16, S17, and S19) remained in SDA and both the AMI and SMI tracked their dynamics as well.

Slow-Wave Modulation is Present in Surgical Patients with Weakened, Absent, or Dissipating Alpha Waves under Propofol-Mediated Unconsciousness. While a key signature of propofol- and sevoflurane-mediated unconsciousness is the presence of strong alpha waves, these oscillations are often weak, dissipating or absent in elderly patients (14). For the elderly, this limits the utility of an index that tracks the transition from SDA to burst suppression by monitoring alpha wave modulation. In this case, the SMI remains a reliable metric for tracking modulatory dynamics during propofol-mediated unconsciousness. Fig. 5 shows the EEG recorded from a 70-y-old man undergoing a robotic laparoscopic prostatectomy. At approximately 40 min after induction of general anesthesia, his alpha oscillations dissipate (Fig. 5*A*). This led to a detection of very long alpha down-states (Fig. 5*B*) and a drastic decrease in the AMI (Fig. 5*C*). These changes in the AMI suggest an early increase in the effect-site concentration. However, the progression of the slow-wave activity is preserved (Fig. 5*D*) and SMI tracked the progression from SDA to burst suppression and back as well (Fig. 5*E*). If AMI is recalibrated after the loss of alpha power—which is possible by our implementation (*Materials and Methods*)—we believe that the alpha waves would still offer a suitable tracking index. BSP, which detects broadband suppression, indicates that there is no burst suppression in the first half of the surgical session despite the weakening of alpha oscillations (Fig. 5*F*).

We analyzed the EEG recordings of 10 surgical patients in whom unconsciousness during general anesthesia was maintained with propofol who showed either weak, dissipating, or absent alpha oscillations. Five of these patients (cases 22–24, 27, and 29;
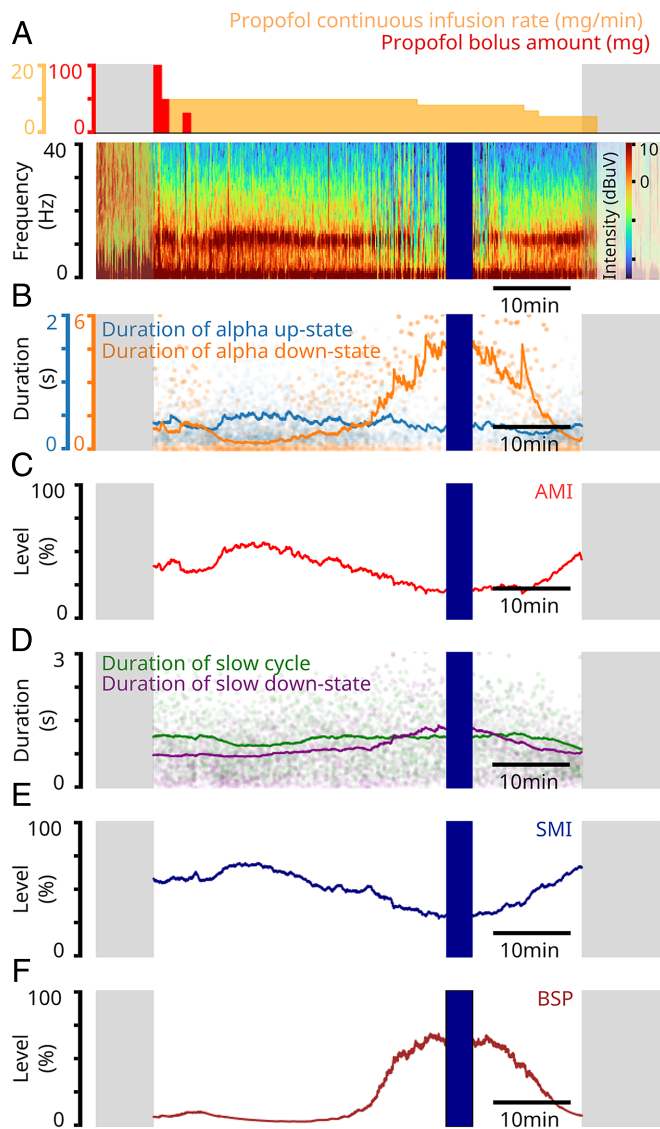
Fig. 4. EEG dynamics of a 44-y-old woman who underwent a laparoscopic cholecystectomy under propofol-mediated unconsciousness show modulation progression from SDA to burst suppression and back to SDA. (*A*) *Top*. Graph showing the propofol administration scheme, combining boluses (red) and continuous infusion (orange). *Bottom*. EEG spectrogram. The dark-blue band is a period of missing EEG data. (*B*) Time series plots showing the alpha up-state (blue) and down-state (orange) durations. The smooth traces are Kalman filter estimates of the corresponding mean state durations. (*C*) Time course of the AMI. See *Text* for definition. (*D*) Time series plots showing the slow-oscillation cycle durations (green) and the slow-oscillation down-state durations (purple). The smooth traces are Kalman filter estimates of the corresponding mean state durations. (*E*) Time course of the SMI. See *Text* for definition. (*F*) Time course of the BSP.

see *SI Appendix*, Figs. S22–S24, S27, and S29) remained in SDA without going into burst suppression, as indicated by their raw EEG traces and their near zero BSP values. In these cases, we often observed sudden weakening or dissipation of the alpha oscillations with concomitant AMI drops at those timepoints suggesting a higher effect-site concentration consistent with burst suppression, while none is present. However, SMI remains at levels comparable to those prior to alpha dissipation. The remaining five patients (cases 21, 25, 26, 28, and 30; see *SI Appendix*, Figs. S21, S25, S26, and S30) show light periods of burst suppression, preceded by alpha oscillation weakening and an early decrease of AMI relative to SMI. An overall decrease

in AMI compared to SMI when alpha waves are weak can be observed when comparing *SI Appendix*, Fig. S41*C* to *SI Appendix*, Fig. S41*B*.

Alpha- and Slow-Wave Modulation are Present in Surgical Patients under Sevoflurane-Mediated Unconsciousness. We predict that the modulatory dynamics observed for propofol would be present for other GABAergic anesthetics, as all the GABAergic anesthetics have similar spectral patterns. Therefore, we analyzed the EEG recordings of 10 surgical patients receiving general anesthesia in whom unconsciousness was maintained with sevoflurane (Fig. 6 *A–F*).
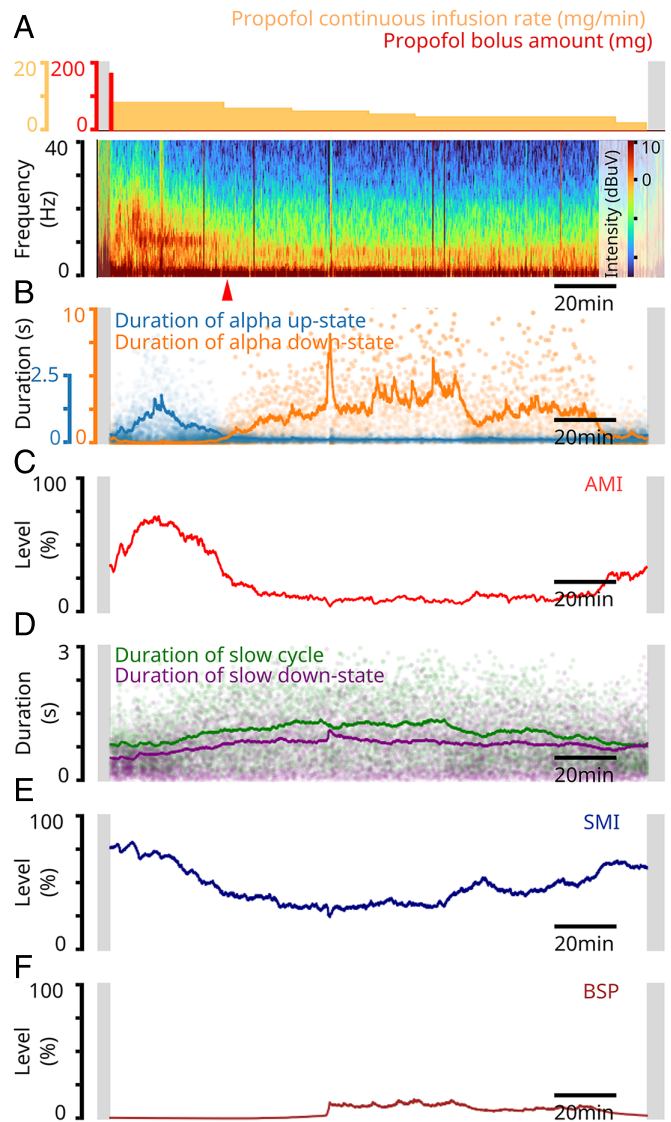

Fig. 5. EEG dynamics of a 70-y-old man who underwent a robotic laparoscopic prostatectomy under propofol-mediated unconsciousness show dissipation of alpha oscillations. (*A*) *Top*. Graph shows the manual propofol infusion scheme, with boluses (red) and continuous infusion (orange). *Bottom*. EEG spectrogram shows a loss of alpha power (red arrow) approximately 30 min after the start of the recording. (*B*) Time series plots showing the alpha up-state (blue) and down-state (orange) durations. The smooth traces are Kalman filter estimates of the corresponding mean state durations. (*C*) Time course of the AMI. See *Text* for definition. (*D*) Time series plots showing the slow-oscillation cycle durations (green) and the slow-oscillation down-state durations (purple). The smooth traces are Kalman filter estimates of the corresponding mean state durations. (*E*) Time course of the SMI. See *Text* for definition. (*F*) Time course of the BSP.

Six of these patients (cases 31–33, 37, 39, and 40; see *SI Appendix*, Figs. S31–S33, S37, S39, and S40) transitioned from SDA into burst suppression and back to SDA. AMI and SMI tracked these transitions. In two of these six cases (cases 31 and 40; see *SI Appendix*, Figs. S31 and S40), the appearance of burst suppression coincides with the administration of propofol boluses indicating a sudden increase of GABAergic anesthetic effect-site concentration. In the other cases (cases 32, 33, 37, and 39; see *SI Appendix*, Figs. S32, S33, S37, and S39), the transition into burst suppression occurs on a high sevoflurane dose, and hence, a high effect-site concentration. This shows, as expected, that this transition does occur when sevoflurane is the primary hypnotic. The remaining four patients (cases 34–36 and 38; see *SI Appendix*,

Figs. S43–S36 and S38) remained in SDA, and AMI and SMI tracked these dynamics.

The Progression of Alpha- and Slow-Wave Modulation Signals a Transition from a Neurophysiological to a Metabolic Anesthetic Effect in the Brain. We build on the biophysical models for alpha oscillations (6, 17), slow-delta oscillations (18), and burst suppression (4) to offer a neural circuit description of how alpha-wave amplitude and slow-wave frequency modulation define the transition from SDA to burst suppression as a function of increasing effect site concentration of a GABAergic anesthetic. Our model is a cortical network consisting of excitatory pyramidal neurons and inhibitory interneurons (*SI Appendix*, Fig. S42) (*Materials and Methods*). Although directly combining the existing biophysical models will produce SDA and burst suppression, this configuration alone is insufficient to produce alpha-wave amplitude and slow-wave frequency modulation. The key insight that our analysis uncovered is that the duration of a slow-wave cycle changes throughout the transition from SDA to burst suppression. If the slow oscillation is dynamically constructed by an interaction of different GABAergic-anesthetic-dependent mechanisms, particularly during SDA, then the modulation processes emerge from the augmented model.

For the purpose of presentation, we describe the formation of the modulation processes in three stages. In the first stage, the effect-site concentration of the GABAergic anesthetic reaches a level sufficient to produce alpha and slow-delta oscillations (Fig. 7, *a*). Its widespread actions also facilitate global inhibition of cortical activity, triggered by a momentary increase in cortical activity and enabled potentially through cortical–thalamic interactions. The global inhibition hyperpolarizes the membranes of the excitatory neurons which manifests as increasingly larger troughs in the slow oscillations and interruption of alpha oscillations by interrupting neuronal spiking activity. The first signs of alpha and slow-wave modulation appear in the EEG (Fig. 7, *a*). In the second stage, as the effect-site concentration of the GABAergic anesthetic continues to increase, global inhibition is further facilitated. As it is triggered more frequently, large slow-wave cycles and alpha oscillation disruption become more frequent. These effects appear as a more profound modulation with increasing slow-wave cycle duration and shorter alpha oscillation up-states (Fig. 7, *b–d*). At the same time, ATP production starts to decline as the GABAergic anesthetic begins to disrupt oxidative phosphorylation in the mitochondrial membranes of the neurons (Fig. 7, *c* and *d*). In the third stage, ATP production is severely impaired so that neuronal spiking activity readily depletes ATP levels thereby forcing inward rectifier ATP-dependent potassium channels to open (*SI Appendix*, Fig. S42). The opening of these channels hyperpolarizes the neurons and enhances the suppression periods observed in both the slow and alpha oscillations. As the GABAergic anesthetic effect-site concentration increases further, the recovery of adequate ATP levels slows more leading to longer suppression periods, which manifest as longer alpha- and slow-wave down-states (Fig. 7, *d–g*) and eventually, burst suppression (Fig. 7, *f* and *g*). The biophysical model output (Fig. 7) captures well the dynamics present in the EEG signals (Fig. 2).

Through our data and modeling analyses, we find that burst suppression is the extreme of alpha-wave amplitude modulation and slow-frequency modulation (Figs. 1 *B*, *d*; 1 *D*, *d*; and 7, *f* and *g*). However, impaired mitochondrial function (the metabolic effect) need not begin with large doses of the GABAergic anesthetic that are often associated with burst suppression. Our
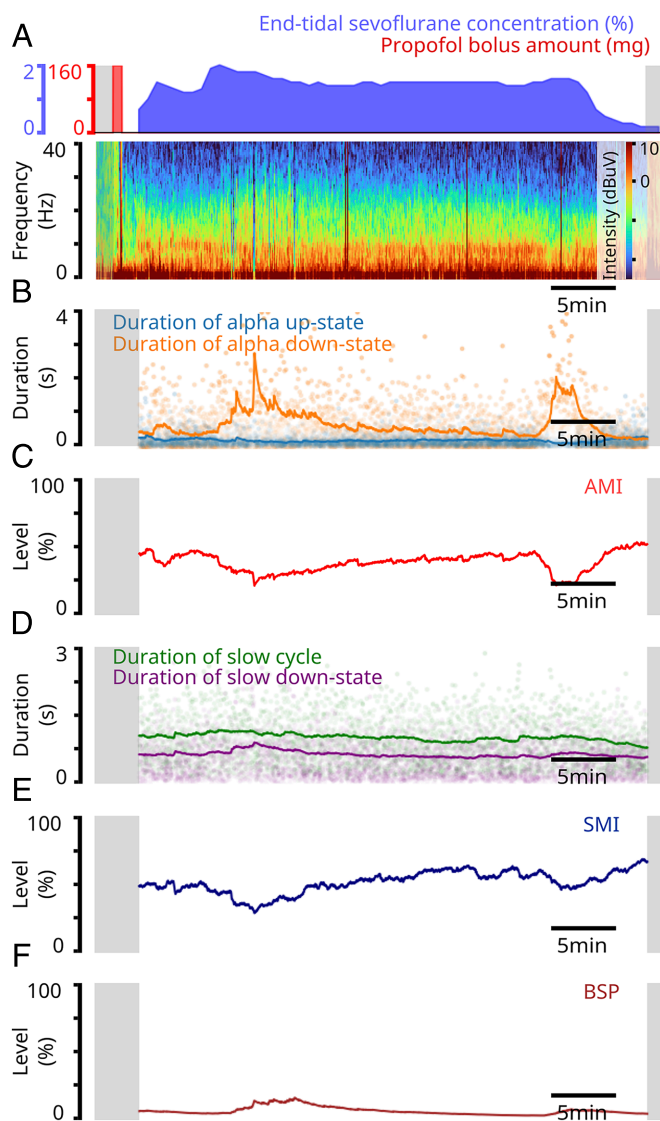

Fig. 6. EEG dynamics of a 54-y-old man who underwent a photoselective vaporization of the prostate under sevoflurane-mediated unconsciousness. (*A*) *Top*. Graph shows the time course of the end-tidal sevoflurane concentration (blue), following a propofol bolus (red) administered for induction. Bottom. Spectrogram of the raw EEG signal. (*B*) Time series plots showing the alpha up-state (blue) and down-state (orange) durations. The smooth traces are Kalman filter estimates of the corresponding mean state durations. (*C*) Time course of the AMI. See *Text* for definition. (*D*) Time series plots showing the slow-oscillation cycle durations (green) and the slow-oscillation down-state durations (purple). The smooth traces are Kalman filter estimates of the corresponding mean state durations. (*E*) Time course of the SMI. See *Text* for definition. (*F*) Time course of the BSP.
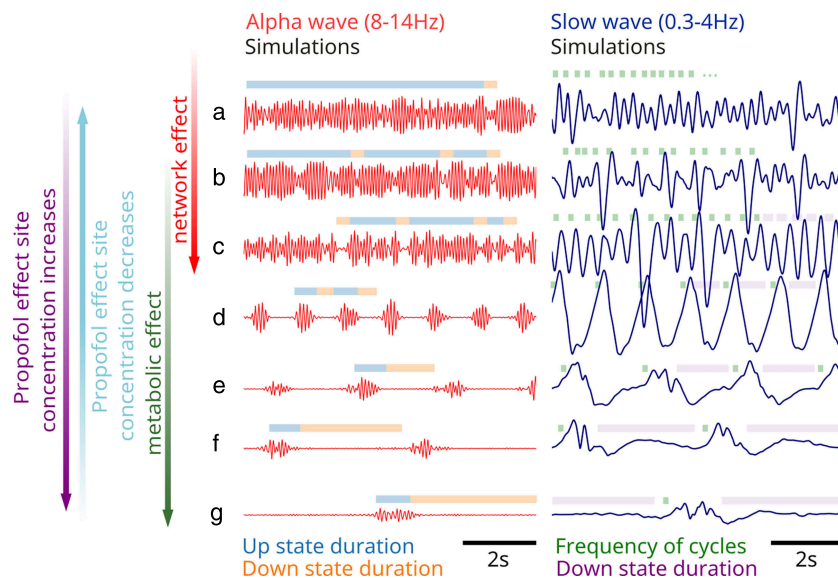
Fig. 7. Biophysical model characterizing the progression from SDA to burst suppression. EEG traces bandpassed filtered in the alpha oscillation range (red) and in the slow-delta oscillation range (blue) obtained by simulating our network model at increasing propofol target effect-site concentrations and neural metabolic effects. A blue bar indicates an alpha-wave up-state and an orange bar indicates alpha-wave down-state. A green square indicates the onset of a slow oscillation cycle, and a purple bar indicates a down-state. The changes in parameters to go from a to g are given in Table 1 in *Materials and Methods*.

modeling analysis suggests that the metabolic effect is present when the alpha-wave down-states and the slow-wave troughs begin to lengthen (Fig. 7, *d* and *e*). These events occur well in advance of the appearance of burst suppression in the EEG. As ATP production becomes more impaired, the metabolic effect manifests prominently as the transition into burst suppression.

Our cortical network produces SDA when there is sufficient binding of the GABAergic anesthetic to the GABA receptors. As the effect-site concentration increases, the slow-delta and alpha oscillations undergo, respectively, frequency- and amplitude-modulation, which coalesce into burst suppression due to the combined neurophysiologic and metabolic effects of the anesthetic (Fig. 7).

Discussion

Alpha-Wave and Slow-Wave Modulation Continuously Track the Transition from SDA Oscillations to Burst Suppression and Back to SDA Oscillations. EEG SDA oscillations and burst suppression are established markers of unconsciousness mediated by GABAergic anesthetics. Burst suppression indicates a more profound state of brain inactivation. We discovered that alpha-wave amplitude modulation and slow-wave frequency modulation track the transition from SDA oscillations to burst suppression and the transition from burst suppression to SDA oscillations as a function of an increasing and decreasing propofol effect site concentrations, respectively.

In our up-down state analysis of the alpha and slow modulations, we discovered two components for both processes. The transition from SDA to burst suppression is marked by shortening of the alpha up-states followed by lengthening of the alpha down-states. During the same transition, the wide slow cycles first become more frequent. Next, the troughs of these cycles lengthen and flatten into long suppression intervals. Our biophysical model suggests that the first component of the two modulatory processes is a neurophysiological effect, whereas the second component is most likely a metabolic effect.

We derived two indices, AMI and SMI, to track, respectively, the alpha and slow modulations during the SDA-burst

suppression-SDA transitions. The indices tracked these dynamics in human volunteers receiving propofol and in actual surgical patients receiving either propofol or sevoflurane as the GABAergic hypnotic agent during general anesthesia. The SMI tracked the changes in dynamics even in the absence or loss of the alpha oscillations, states that commonly occur in elderly patients. Because both indices track the SDA-burst suppression-SDA transition, we infer that both track changes in level of unconsciousness. Our biophysical model supports this inference as it shows that the modulatory processes which these indices track are generated by the combined neurophysiological and metabolic effects of GABAergic anesthetics on neural circuits. An important caveat is that none of the volunteers or patients received ketamine, an agent known to alter the EEG signatures of GABAergic anesthetics (19, 20).

Prior Studies of Alpha- and Slow-Wave Modulation. Schroeder and Barr (21) studied EEG alpha oscillation modulation in a nonanesthesia context and used the term amplitude modulation index in their analyses. Because we studied the same dynamics, albeit with different algorithms, we used the same term. Shao and colleagues (14) established a correlation between low frontal alpha power and the propensity to observe burst suppression during propofol- and sevoflurane-mediated unconsciousness in the elderly. They proposed decreased brain energy stores in elderly patients made worse by anesthetic inhibition of brainstem excitatory neuromodulation as a possible mechanism for this correlation. Cartailler and colleagues (13) showed that alpha suppression during the early stages of propofol-mediated unconsciousness was a predictor of the subsequent appearance of burst suppression. Our data analysis and biophysical modeling suggest that low-amplitude alpha oscillations and early evidence of alpha suppression could be due to an earlier onset of the metabolic effects of the GABAergic anesthetic.

Modulation of the alpha oscillation by the slow oscillation has been reported in two forms for propofol: trough-max and peak-max (3, 12, 22). In the former, identified as a marker of both loss and recovery of consciousness, the amplitude of the alpha

oscillation is maximal at the trough of the slow oscillation. In the latter, identified as a marker of unconsciousness, the amplitude of the alpha oscillation is maximal at the peak of the slow oscillation. That is, during peak-max, the alpha up-states are reported to co-localize with the up-cycle in the slow oscillation. During the immediate pre-burst suppression and burst suppression states, we observed this co-localization (*SI Appendix*, Fig. S43 *A* and *B*). However, in the transition to burst suppression, we found that the slow oscillation troughs changed with increasing anesthetic dose and did not always signify a down-state for the alpha oscillations (Fig. 7). Our biophysical modeling shows that the slow oscillation shape and period are formed dynamically as a function of increasing GABAergic anesthetic dose, due to its combined neurophysiological and metabolic effects (Fig. 7). The metabolic effects lengthen both the alpha and the slow oscillation down-states. The two down-states eventually overlap and devolve into suppression periods. Our model suggests that suppression of spiking activity should accompany the suppression periods. Indeed, in our nonhuman primate studies of propofol-mediated unconsciousness, we observed suppression of spiking activity during the suppression periods in the local field potentials (8).

Mechanisms for the Combined Neurophysiological and Metabolic Effects of GABAergic Anesthetics.

Our data analyses and modeling link EEG alpha- and slow-wave modulation to neurophysiological and metabolic effects of GABAergic anesthetics. The presence of the slow, delta and alpha oscillations represents principally a neurophysiological effect, whereas progression into the alpha and slow modulations represents the neurophysiological effect and the progression of the metabolic effect. Burst suppression is the extreme presence of the modulatory effect. The modulations suggest that the metabolic effects of the GABAergic anesthetics begin well in advance of burst suppression. However, it is not possible to determine exactly when the metabolic effects emerge using only our data, without additional experiments. Our biophysical model builds on the alpha oscillation model proposed by Ching and colleagues (6), the slow oscillation model proposed by Soplata and colleagues (18), and the burst suppression model designed by Ching and colleagues (4).

There is substantial experimental evidence to support possible mechanisms for the metabolic effects we propose. Positron emission tomography studies in humans show that administering propofol decreases $CMRO_2$ and cerebral blood flow (23, 24). Findings from in vitro studies show that GABAergic anesthetics slow ATP production by abolishing mitochondrial membrane potentials (25) and, thereby, blocking the conversion of ADP to ATP. In addition, experiments have shown that GABAergic anesthetics act on mitochondrial respiratory enzymes (26–28) leading to a decrease in oxygen consumption and inducing a switch to glycolysis. As noted above, Shao and colleagues (14) proposed a circuit mechanism for the higher propensity of burst suppression in elderly patients. Their hypothesis could be extended to explain in part the contributions of metabolic effects to the modulatory dynamics in older patients. These possible mechanisms are not mutually exclusive and can certainly act in concert.

Implications of AMI and SMI for Monitoring Unconsciousness and Brain Metabolic State.

AMI and SMI can be computed and displayed in real time as measures of unconsciousness for a patient in whom a GABAergic anesthetic is the primary agent maintaining unconsciousness. These indices contain the information in the BSP as a special case. Hence, this suggests that AMI and SMI could be used clinically to monitor unconscious during general anesthesia. As real time markers of unconsciousness, they could also be used to implement a system for closed-loop control of anesthetic state in either the operating room or in the intensive care unit. We restate that we propose these applications of AMI and SMI with the proviso that ketamine is not being coadministered to help maintain general anesthesia or sedation (19, 20).

In future work, we will test experimentally the metabolic hypothesis proposed by our biophysical model by measuring simultaneously neurophysiological responses and metabolic responses during controlled upward and downward titrations of propofol or another GABAergic anesthetic. If the relationship between the indices, the neurophysiological and the metabolic responses, is correct then the indices could also be used to track the metabolic state of a patient in the operating room or in the intensive care unit. A more accurate characterization of brain state could lead to more judicious anesthetic dosing and a possible reduction in postoperative cognitive disorders (29–31). It may also enable more precise anesthetic titration to maintain a desired level of neuroprotection for patients placed in a medical coma to treat status epilepticus or to control intracranial hypertension. Our characterization of the modulatory dynamics mediated by GABAergic anesthetics during transitions between states of unconsciousness offers important mechanistic insights that could be readily applied in clinical care.

Materials and Methods

Data Acquisition. All data collection and experimental protocols were approved by the Mass General Brigham Human Research Committee (Institutional Review Board). For the propofol volunteer study, all subjects provided informed consent. For the surgical patient studies, there was no data collection specific consent as the EEG recordings, physiological data, and anesthetic administration data were collected as part of standard care and deidentified.

Volunteer subjects under propofol-mediated unconsciousness. The propofol volunteer dataset–utilized in ref. 3–consists of EEG recordings from 10 healthy volunteers between the ages 18 and 36, American Society of Anesthesiology Physical Status I, and with Mallampati Class I airway anatomy. Safety measures and clinical details are provided in ref. 3.

Propofol was administered via computer-controlled infusion to achieve target effect-site concentrations of 0, 1, 2, 3, 4, and 5 μg/mL, based on a three-compartment pharmacokinetic model of propofol (32). Each target concentration was held for 14 min. Following ref. 32, clearance and volume parameters of the model were adjusted to each volunteer based on their age, sex, height, and weight. The dynamics of other compartments were assumed to be unaffected by the addition of an effect site compartment, with a balanced one-way exchange rate and clearance from the system estimated from ref. 33. In some cases, target effect-site concentrations were decreased in a stepwise fashion, so that both induction and emergence from unconsciousness were gradual. Unconsciousness was determined by the response of a subject to auditory stimuli (clicks or words), which were presented every 4 s. Details of the auditory stimuli are provided in ref. 3. Unresponsiveness to the auditory stimuli was interpreted as unconsciousness. Details of computing the probability of response to auditory stimuli and identifying loss of consciousness and return of consciousness are provided in ref. 3.

Whole head EEG data were recorded using a 64-channel BrainVision MRI Plus system (Brain Products) with a sampling rate of 5,000 Hz, bandwidth 0.016 to 1,000 Hz, and resolution 0.5 μV least significant bit. The Fp1 channel was used for all further analysis. Subjects were instructed to close their eyes throughout the experiment to avoid eye-blink artifacts in the EEG.

Surgical patients under propofol-mediated unconsciousness, with strong alpha waves. This dataset was created from a database of real-time EEG recordings of 140 patients who underwent general anesthesia or monitored anesthesia care between August 1, 2020 and March 1, 2022. Frontal EEG data were recorded using the SedLine brain function monitor (Masimo Corporation, Irvine, CA) with a sampling frequency of 178 Hz. The Fp2 channel was used for

further analysis. A research assistant annotated accurate time points of all drug changes and all OR events, including the patient's arrival, EEG recording start and end times, surgical events, induction, intubation, and extubation.

Ten cases were selected to be included in this dataset if they met the following inclusion criteria: i) The patient underwent general anesthesia. ii) The recording did not exhibit excessive muscle artifacts or electrical impedance from electrocautery. iii) The recording does not exhibit data quality issues characteristic of SedLine as reported in ref. 34. iv) The primary hypnotic agent was propofol. v) The EEG exhibits high alpha band power during unconsciousness. With regards to criterion (iii), Von Dincklage et al. (34) describe the following three main problems in EEG recordings from the SedLine monitors: a) An undocumented change in the sample rate of the recorded EEG due to a change in display feed; b) An undocumented change in the amplitude and quantization of the recorded EEG; and c) Clipping or stair-step-like distortion of the EEG signal that's dependent on the position of the signal on the screen. To address (a) and (b), we ensured that the display feed settings did not change during data collection to prevent undocumented changes in the sample rate, amplitude, and quantization. To address (c), we visually inspected the recording to ensure selection of cases without clipping or stair-step-like distortion of the EEG signal.

Surgical patients under propofol-mediated unconsciousness, with weakened, absent, or dissipating alpha waves. This dataset was created in the same way as the dataset for surgical patients under propofol-mediated unconsciousness showing strong alpha waves, with the exception of the last criterion which was substituted with the following: (v) The EEG exhibits low alpha band power, dissipating alpha oscillations or absence of alpha oscillations during unconsciousness.

Surgical patients under sevoflurane-mediated unconsciousness. This dataset was created from a database of real-time EEG recordings of 247 patients who underwent general anesthesia or monitored anesthesia care between November 1, 2011 and August 20, 2015. Clinical information including approximate times of drug changes and events such as induction, intubation, and extubation were collected from the Epic electronic medical record system. Frontal EEG data were recorded using the SedLine brain function monitor (Masimo Corporation, Irvine, CA) with a pre-amplifier bandwidth of 0.5 to 92 Hz, sampling rate of 250 Hz, and with 16-bit, 29 nV resolution. The Fp2 channel was used for further analysis.

Ten cases were selected to be included in this dataset if they met the following inclusion criteria: i) The patient underwent general anesthesia. ii) The recording did not exhibit excessive muscle artifacts or electrical impedance from electrocautery. iii) The primary hypnotic agent was sevoflurane. iv) The EEG exhibits high alpha band power during unconsciousness.

Filtering and Signal Processing. EEG polarity was adjusted so that the initial burst of activity during burst suppression corresponded to positive deflections, corresponding with spiking activity in NHP studies (8). All EEG spectrograms for visualization were computed using the multitapered method (35). The alpha and slow oscillations were obtained from the raw EEG by band-pass filtering between 8 and 14 Hz (alpha) and 0.3 to 4 Hz (slow-delta), respectively, using a second-order Butterworth filter.

A state-space Gaussian Kalman filter was implemented to derive estimates of the durations utilized in AMI and SMI, in an online manner for real-time computation. Let y and x denote, respectively, the observation and its corresponding latent state that needs to be estimated. The state and observation equations were defined as:

$$x_{n+1} = x_n + v_n \Delta t \tag{1}$$
$$y_n = x_n + \epsilon_n \tag{2}$$

where Δt is the EEG sampling period, and $v_n \sim \mathcal{N}(0, \sigma_v^2)$ and $\epsilon_n \sim \mathcal{N}(0, \sigma_\epsilon^2)$ are independently and identically drawn (iid) from gaussian distributions. Let $x_{n|m}$ and $\sigma_{n|m}^2$ denote the state at time n and its corresponding variance, respectively, estimated from the observations $y_0, \cdots, y_m$. The one-step Kalman prediction equations become

$$x_{n|n-1} = x_{n-1|n-1} \tag{3}$$
$$\sigma_{n|n-1}^2 = \sigma_{n-1|n-1}^2 + \Delta t^2 \sigma_v^2. \tag{4}$$

The Kalman gain is

$$K_n = \frac{\sigma_{n|n-1}^2}{\sigma_{n|n-1}^2 + \sigma_\epsilon^2} \tag{5}$$

and the Kalman update equations become

$$x_{n|n} = x_{n|n-1} + K_n(y_n - x_{n|n-1}) \tag{6}$$
$$\sigma_{n|n}^2 = (1 - K_n)\sigma_{n|n-1}^2 \tag{7}$$

Initial conditions $x_{0|0}$ and $\sigma_{0|0}^2$ for filtering were computed by running the Kalman filter on the reversed signal, namely $y[M - n]$ where M is the length of y. The initial conditions can instead be determined, with no changes to the resulting filtered traces, by computing the mean of y_n and the variance of $y_n - y_{n-1}$ in a time window around the initial time.

In our equations, the Kalman gain K_n quickly converges to K (36) satisfying $(1 - K)\Delta t^2 \sigma_v^2 = K^2 \sigma_\epsilon^2$, and the interpretation of our Kalman filtering coincides with applying a first-order low-pass filter with cut-off frequency of $Kf_s/2\pi$ where f_s denotes the sampling frequency. We adjust the cut-off frequency to coincide with a period of 5 min ($D = 300$ s), to focus on the variations at that temporal scale. For AMI-related computation, we set σ_v and σ_ϵ to be any pair that satisfies $(1 - \lambda)\Delta t^2 \sigma_v^2 = \lambda^2 \sigma_\epsilon^2$ with $\lambda = 2\pi/(Df_s)$. In this setting, λ coincides with the steady state Kalman gain. For SMI-related computations, we scale the observation noise variance by a factor of 10. In general, by changing λ (via D), one can control the smoothness of the filtered curves.

For the volunteer and sevoflurane subjects ($1/\Delta t = 250$ Hz), we fixed $\sigma_\epsilon = 1$ and $\sigma_v = 0.0209$ for AMI, and $\sigma_\epsilon = 10$ and $\sigma_v = 0.0209$ for SMI. For the propofol surgical subjects ($1/\Delta t = 178$ Hz), we fixed $\sigma_\epsilon = 1$ and $\sigma_v = 0.0207$ for AMI and $\sigma_\epsilon = 10$ and $\sigma_v = 0.0207$ for SMI. Most importantly, these parameters were fixed to be the same for all subjects in their respective category, depending on EEG sampling frequency.

An alternative approach would be to determine σ_ϵ^2 and σ_v^2 using an EM algorithm with prior distributions on σ_ϵ^2 and σ_v^2 (15).

Both AMI and SMI use the same calibration 300 s window to determine the modulation thresholds. See the following subsections on AMI and SMI computation for more details.

AMI Computation. The alpha oscillation EEG_{alpha} was obtained by band-pass filtering between 8 and 14 Hz using a second-order Butterworth filter. The goal was to fix a modulation threshold M and determine when the upper envelope of EEG_{alpha} is above or below M, indicating a period of up-state or down-state, respectively.

For a fixed modulation threshold, the up-/down-states were determined as follows. All the peaks of the absolute value signal $|EEG_{alpha}|$ above M were determined, and any time point within 50 ms (half the period of a 10 Hz oscillation) of such a peak was considered to be in an alpha up-state. The remaining time points corresponded to an alpha down-state. A peak in $|EEG_{alpha}|$ was detected at time point k if $|EEG_{alpha}|$ at time points $k - 1$ and $k + 1$ had values lower than that at time point k.

For a calibration window of 300 s, the modulation threshold M was determined as the 50th percentile of the amplitudes of all the peaks of EEG_{alpha} within that calibration window. This choice is designed to roughly yield up- and down-states of similar durations during the calibration period. The peaks in EEG_{alpha} in the calibration window were similarly detected as done for $|EEG_{alpha}|$.

The durations of all up-states and down-states were computed. The computed durations appear in panel B, as blue and orange scatter plots, of all data figures. A signal for the up-state duration was formed by setting the value between the start of an up-state and the start of a next one (following a down-state) to be the duration of that first up-state. A similar down-state duration signal was derived, considering down- instead of up-states.

Real-time versions of the duration signals, for use as real-time observations in the AMI computation, that do not depend on future information were derived as follows. The observed duration of an alpha up-state at time n corresponds to the maximum between the duration of the current up-state until time n (if at time n, alpha oscillations are in an up-state) and the duration of the last alpha up-state.

If at time n, alpha oscillations are in a down-state, then the observed duration is the duration of the last up-state. The signal was defined similarly for down-states. These signals were then passed through a Kalman filter for estimating the latent state duration, to yield two duration signals d_{up} and d_{down}, which also appear in panel B of all data figures.

An EEG signature was derived as $s_{alpha} = \log(d_{up}/d_{down})$ which tracks the evolution of the duration of up- and down-states, and the marker was derived by applying a logistic function on s_{alpha}, specifically $\frac{1}{1+\exp(-\gamma s_{alpha})}$, which yields

$$AMI = \frac{d_{up}^{\gamma}}{d_{up}^{\gamma} + d_{down}^{\gamma}}. \qquad [8]$$

The quantity γ dictates the dynamic range of AMI and how quickly AMI saturates near 0 or 1. We set $\gamma = 0.5$ for AMI throughout the study. This value can be modified as needed depending on the situation.

Our Kalman filtering assumes that the noise term $\epsilon_n = y_n - x_n$ is independently and identically distributed. In filtering for alpha up-state durations, the observation y_n is fixed during an alpha down-state, yielding correlated observations. However, the state variable of the up-state duration can still vary. Indeed, anesthetic effect site concentration can continue to increase or decrease during a down-state, altering the length of the next up-state which is not yet observable. Therefore, throughout the assumed process, $y_n - x_n$ is not correlated by design, and therefore, the iid assumption is satisfied.

While the evolution for alpha up- and down-states have been obtained separately through Kalman filtering, after which AMI is computed, it is possible to combine these observations into one estimation framework. Indeed, AMI results from applying a logistic function onto the signature $s_\alpha = \log(d_{up}/d_{down})$. It is then possible to derive corresponding linear state and observation equations from $s_\alpha = \log(d_{up}) - log(d_{down})$, upon which to apply Kalman filtering, and directly estimate AMI. This approach is a subject of future work.

Additional practical considerations for AMI computation are detailed in *SI Appendix*.

SMI Computation. The slow oscillation EEG_{slow} was obtained by band-pass filtering between 0.3 and 4 Hz using a second-order Butterworth filter. The goal was to fix two modulation thresholds M_C (crossing) and M_Q (quiescence), with $M_C < M_Q$ and determine the duration of a slow oscillation cycle in EEG_{slow} each detected by crossings at M_C and the duration of the down-states, being the periods of EEG_{slow} below M_Q.

To determine the duration of a slow oscillation cycles in EEG_{slow}, the time points where EEG_{slow} crosses M_C were determined and EEG_{slow} was segmented into cycles delimited by three crossings: a first crossing from below M_C that indicated the start of a cycle, a mid crossing from above M_C, and a final crossing from below M_C that indicated the end of a cycle. Each cycle then consisted of a positive deflection followed by a negative deflection. The duration of all cycles was determined, and two signals, one for the cycle duration and one for the frequency of cycles, were derived by setting the value at a time point equal to the duration (or frequency) of the cycle it belongs to. The computed cycle durations are shown in a green scatter plot in panel D of all data figures.

Real-time versions of the cycle duration and frequency signal, for use as observation signal in the SMI computation, that do not depend on future information were derived as follows. The observed duration of a slow cycle at time n corresponds to the maximum between the duration of the current slow cycle until time n and the duration of the last slow cycle. The signal was defined similarly for the frequency of cycles observation. These signals for the cycle duration and cycle frequency were passed through a Kalman filter to yield two signals d_{slow} and f_{slow}. The signal d_{slow} appears in panel D of all data figures.

To determine the duration of the down-states in EEG_{slow}, all time points with values below M_Q were considered to belong to a down-state. The different durations of the down-states were determined, and a down-state duration signal was formed by setting the value at the time point to be the duration of its corresponding down-state if it was during one, or the duration of the previous down-state if it does not belong to one. Real-time observation signal were derived as performed for the cycle duration and frequency above, then Kalman filtered to yield a signal $d_{suppression}$, which appears in panel D of all data figures.

For a calibration window of 300 s, we determined M_C by a parameter sweep, choosing the threshold that maximizes the number of crossings in that window. Note that M_C has a value near 0 given the bandpass filtering between 0.3 and 4 Hz to obtain the slow wave. To determine M_Q, we find a threshold $M' > M_C$ in that calibration window such that the frequency of crossings is reduced by 30%, and then slightly lower that threshold, e.g., by defining $M_Q = 0.5M_C + 0.5M'$. The suppression periods during burst suppression will fluctuate around M_C, and the definition of M_Q is to ensure that they are detected by raising the threshold M_C to one that reduces crossing, and then lowering it again to ensure that it does not erroneously detect low-amplitude nonsuppression slow cycles. Other threshold calibration schemes, or detection methods, are also possible, and can be a subject of future research.

An EEG signature was derived as

$$s_{slow} = \log\left(\frac{f_{slow}/\bar{f}_{slow}}{d_{suppression}/\bar{d}_{suppression}}\right)$$

where $\bar{f}_{slow}$ and $\bar{d}_{suppression}$ denote the average over the calibration window of the crossing frequency and down-state duration, respectively. The signature tracks the evolution of the slow oscillation dynamics, and the marker was derived by applying a logistic function on s_{slow}, specifically $\frac{1}{1+\exp(-\gamma s_{slow})}$, which yields

$$SMI = \frac{(f_{slow}/\bar{f}_{slow})^{\gamma}}{(f_{slow}/\bar{f}_{slow})^{\gamma} + (d_{suppression}/\bar{d}_{suppression})^{\gamma}}. \qquad [9]$$

Similar to the case of AMI, the quantity γ dictates the dynamic range of SMI, and how quickly SMI saturates near 0 or 1. We set $\gamma = 2$ for SMI throughout the study. This value can be modified as needed depending on the situation.

Similar to what was suggested for AMI computation, it is also possible to combine the two observations for SMI into one estimation framework. This approach is a subject of future work.

Additional practical considerations for SMI computation are detailed in *SI Appendix*.

BSP Computation. The BSP computation is derived from ref. 15 and adapted to the analysis in this paper. A state-space algorithm was implemented to derive BSP. Details of the algorithm are provided in *SI Appendix*.

Biophysical Modeling. Our biophysical model consisted of interconnected 80 pyramidal neurons (PYR) and 20 fast-spiking interneurons (FS). All neurons are modeled using a single compartment with Hodgkin–Huxley-type dynamics. The voltage change dv/dt in each cell with membrane capacitance c_m is described by

$$c_m \frac{dv}{dt} = -\sum I_{membrane} - \sum I_{synaptic} + I_{app} + I_{noise}.$$

All cells display a fast sodium current (I_{Na}), a fast potassium current (I_K), and a leak current (I_L) for membrane currents ($I_{membrane}$). PYR additionally displayed an ATP-gated potassium current (4, 37) that captures the metabolic effect and a global inhibitory current that captures inhibitory facilitation of the corticothalamic system. The synaptic currents ($I_{synaptic}$) depend on the connectivity. Details on the modeling are provided in *SI Appendix*.

Adenosine triophosphate (ATP)-gated potassium current. This current is adapted from refs. 4 and 37 and encapsulates the metabolic effect on neurons. It is defined as

$$I_{K_{ATP}} = g_{K_{ATP}} z(V - E_k) \text{ with } z = \frac{1}{1 + 10[ATP]} \qquad [10]$$

and governed by the following two equations:

$$[\dot{Na}] = FI_{Na} - 3K_m[Na]^3[ATP] \qquad [11]$$

$$[\dot{ATP}] = J_{ATP}([ATP]_{max} - [ATP]) - K_m[Na]^3[ATP] \qquad [12]$$

The value of J_{ATP} governs the rate of ATP production and was decreased as propofol concentration increased, as a proxy for metabolic impairment. Low levels of ATP will open up the K_{ATP} channels which hyperpolarizes the cell. The cell is then in a state of suppression until ATP levels replenish. That duration lengthens as the production rate is impaired (see *SI Appendix* for more details).

Global thalamocortical inhibition current. This current encapsulates the neurophysiological effect on neurons during the modulation and is defined as

$$I_{global} = g_{global} v \qquad [13]$$

with $g_{global} = 0.1\ \mu A \cdot cm^{-2}$ and

$$\dot{v} = -0.001v + \frac{1}{1 + \exp[-10(\sum_n [Na] - L_{global})]}. \qquad [14]$$

The quantity $\sum_n [Na]$ is summed over all PYR neurons, as a proxy for the aggregate activity in the network, that will trigger the global inhibition. The threshold L_{global} was decreased as propofol concentration increased. Synchronous high activity in cortex triggers a surge of inhibition or disexcitation through the corticothalamic system, that lead to a momentary shutdown of activity (see *SI Appendix* for more details). A full corticothalamic biophysical implementation of the global inhibition current can be achieved by incorporating a thalamic model of thalamocortical (TC) and reticular (RE) cells (6, 18). In particular, depolarization of TC cells can switch the thalamus out of bursting mode to yield a momentary down-state in thalamic activity (18). This depolarization can be triggered by a synchronous surge of cortical activity (18, 38) and a mechanism of how thalamocortical feedback could influence the EEG as a function of propofol effect-site concentration is elaborated in ref. 38.

Aggregate activity, simulations, and analysis. The aggregate population activity, from which spectral information was determined, consisted of the sum of the membrane potentials of the PYR cells. Our simulations only altered the parameters J_{ATP} and L_{global} to represent different effect site concentrations. The exact values are given in Table 1. Details on all the model parameters are given in *SI Appendix*.

Our network model was programmed in C++ and compiled using GNU gcc. The differential equations were integrated using a fourth-order

Table 1. Simulation parameters for Fig. 7

EEG trace	a	b	c	d	e	f	g
L_{global}	16	15	14	14	14	14	14
J_{ATP}	0.04	0.04	0.024	0.008	0.004	0.0024	0.0016

Runge–Kutta algorithm, with integration time step of 0.05 ms. The model output was analyzed using Python 3.

Author affiliations: [a]Picower Institute for Learning and Memory, Department of Brain and Cognitive Sciences, Massachusetts Institute of Technology, Cambridge, MA 02139; [b]Department of Anesthesia, Critical Care and Pain Medicine, Massachusetts General Hospital, Boston, MA 02114; and [c]Department of Anaesthesia, Harvard Medical School, Boston, MA 02115

Author contributions: E.N.B. and E.A. proposed the conceptual framework; E.A., O.K., K.A.M., and E.N.B. designed the research; E.A., O.K., and K.A.M. performed the research with input from E.N.B; O.K. and E.N.B collected the surgical data; and E.A., E.N.B., O.K., and K.A.M. wrote the paper.

Competing interest statement: E.N.B holds patents on anesthetic state monitoring and control. E.N.B. holds founding interest in PASCALL, a start-up developing physiological monitoring systems; receives royalties from intellectual property through Massachusetts General Hospital licensed to Masimo. The interests of E.N.B. were reviewed and are managed by Massachusetts General Hospital and Mass General Brigham in accordance with their conflict of interest policies.

1. P. L. Purdon, A. Sampson, K. J. Pavone, E. N. Brown, Clinical electroencephalography for anesthesiologists. Part I: Background and basic signatures. *Anesthesiology* **123**, 937–960 (2015).
2. E. N. Brown, K. J. Pavone, M. Naranjo, Multimodal general anesthesia: Theory and practice. *Anesth. Analg.* **127**, 1246–1258 (2018).
3. P. L. Purdon et al., Electroencephalogram signatures of loss and recovery of consciousness from propofol. *Proc. Natl. Acad. Sci. U.S.A.* **110**, E1142–E1151 (2013).
4. S. Ching, P. L. Purdon, S. Vijayan, N. J. Kopell, E. N. Brown, A neurophysiological-metabolic model for burst suppression. *Proc. Natl. Acad. Sci. U.S.A.* **109**, 3095–3100 (2012).
5. A. Shanker, J. H. Abel, G. Schamberg, E. N. Brown, Etiology of burst suppression EEG patterns. *Front. Psychol.* **12**, 673529 (2021).
6. S. Ching, A. Cimenser, P. L. Purdon, E. N. Brown, N. J. Kopell, Thalamocortical model for a propofol-induced α-rhythm associated with loss of consciousness. *Proc. Natl. Acad. Sci. U.S.A.* **107**, 22665–22670 (2010).
7. F. J. Flores et al., Thalamocortical synchronization during induction and emergence from propofol-induced unconsciousness. *Proc. Natl. Acad. Sci. U.S.A.* **114**, E6660–E6668 (2017).
8. A. M. Bastos et al., Neural effects of propofol-induced unconsciousness and its reversal using thalamic stimulation. *eLife* **10**, e60824 (2021).
9. J. An et al., Variability in pharmacologically-induced coma for treatment of refractory status epilepticus. *PLoS ONE* **13**, e0205789 (2018).
10. E. Mahanna-Gabrielli et al., State of the clinical science of perioperative brain health: Report from the American Society of Anesthesiologists Brain Health Initiative Summit 2018. *Br. J. Anesth.* **123**, 464–478 (2019).
11. J. C. Belrose, R. R. Noppens, Anesthesiology and cognitive impairment: A narrative review of current clinical literature. *BMC Anesthesiol.* **19**, 1–12 (2019).
12. E. A. Mukamel et al., A transition in brain state during propofol-induced unconsciousness. *J. Neurosci.* **34**, 839–845 (2014).
13. J. Cartailler, P. Parutto, C. Touchard, F. Vallée, D. Holcman, Alpha rhythm collapse predicts iso-electric suppressions during anesthesia. *Commun. Biol.* **2**, 327 (2019).
14. Y. R. Shao et al., Low frontal alpha power is associated with the propensity for burst suppression: An electroencephalogram phenotype for a "vulnerable brain". *Anesth. Analg.* **131**, 1529 (2020).
15. J. Chemali, S. Ching, P. L. Purdon, K. Solt, E. N. Brown, Burst suppression probability algorithms: State-space methods for tracking EEG burst suppression. *J. Neural Eng.* **10**, 056017 (2013).
16. E. N. Brown, R. Lydic, N. D. Schiff, General anesthesia, sleep, and coma. *N. Engl. J. Med.* **363**, 2638–2650 (2010).
17. S. Vijayan, S. Ching, P. L. Purdon, E. N. Brown, N. J. Kopell, Thalamocortical mechanisms for the anteriorization of alpha rhythms during propofol-induced unconsciousness. *J. Neurosci.* **33**, 11070–11075 (2013).
18. A. E. Soplata et al., Thalamocortical control of propofol phase-amplitude coupling. *PLoS Comput. Biol.* **13**, e1005879 (2017).
19. O. Akeju et al., Electroencephalogram signatures of ketamine anesthesia-induced unconsciousness. *Clin. Neurophysiol.* **127**, 2414–2422 (2016).
20. O. Akeju et al., GABAA circuit mechanisms are associated with ether anesthesia-induced unconsciousness. *Clin. Neurophysiol.* **127**, 2472–2481 (2016).
21. M. J. Schroeder, R. E. Barr, An alpha modulation index for electroencephalographic studies using complex demodulation. *Med. Biol. Eng. Comput.* **38**, 306–310 (2000).
22. E. P. Stephen et al., Broadband slow-wave modulation in posterior and anterior cortex tracks distinct states of propofol-induced unconsciousness. *Sci. Rep.* **10**, 1–11 (2020).
23. M. T. Alkire et al., Cerebral metabolism during propofol anesthesia in humans studied with positron emission tomography. *J. Am. Soc. Anesthesiol.* **82**, 393–403 (1995).
24. K. K. Kaisti et al., Effects of sevoflurane, propofol, and adjunct nitrous oxide on regional cerebral blood flow, oxygen consumption, and blood volume in humans. *J. Am. Soc. Anesthesiol.* **99**, 603–613 (2003).
25. Ji. Kishikawa et al., General anesthetics cause mitochondrial dysfunction and reduction of intracellular ATP levels. *PLoS ONE* **13**, e0190213 (2018).
26. R. Bains, M. Moe, M. Vinje, J. Berg-Johnsen, Sevoflurane and propofol depolarize mitochondria in rat and human cerebrocortical synaptosomes by different mechanisms. *Acta Anaesthesiol. Scand.* **53**, 1354–1360 (2009).
27. N. Berndt et al., Possible neurotoxicity of the anesthetic propofol: Evidence for the inhibition of complex ii of the respiratory chain in area CA3 of rat hippocampal slices. *Arch. Toxicol.* **92**, 3191–3205 (2018).
28. C. Sumi et al., Propofol induces a metabolic switch to glycolysis and cell death in a mitochondrial electron transport chain-dependent manner. *PLoS ONE* **13**, e0192796 (2018).
29. T. G. Monk et al., Predictors of cognitive dysfunction after major noncardiac surgery. *J. Am. Soc. Anesthesiol.* **108**, 18–30 (2008).
30. I. Rundshagen, Postoperative cognitive dysfunction. *Dtsch. Ärztebl. Int.* **111**, 119 (2014).
31. J. Moller et al., Long-term postoperative cognitive dysfunction in the elderly: ISPOCD1 study. *Lancet* **351**, 857–861 (1998).
32. T. W. Schnider et al., The influence of age on propofol pharmacodynamics. *J. Am. Soc. Anesthesiol.* **90**, 1502–1516 (1999).
33. T. W. Schnider et al., The influence of method of administration and covariates on the pharmacokinetics of propofol in adult volunteers. *J. Am. Soc. Anesthesiol.* **88**, 1170–1182 (1998).
34. F. von Dincklage, C. Jurth, G. Schneider, P. S. García, M. Kreuzer, Technical considerations when using the EEG export of the SEDLine root device. *J. Clin. Monit. Comput.* **35**, 1047–1054 (2021).
35. B. Babadi, E. N. Brown, A review of multitaper spectral analysis. *IEEE Trans. Biomed. Eng.* **61**, 1555–1564 (2014).
36. L. Ljung, *System Identification* (Springer, 1998).
37. M. Cunningham et al., Neuronal metabolism governs cortical network response state. *Proc. Natl. Acad. Sci. U.S.A.* **103**, 5597–5601 (2006).
38. A. E. Soplata et al., Rapid thalamocortical network switching mediated by cortical synchronization underlies propofol-induced EEG signatures: A biophysical model. *J. Neurophysiol.* **130**, 86–103 (2023).
39. E. Adam, O. Kwon, K. A. Montejo, E. Brown, Electroencephalogram dynamics during unconsciousness mediated by GABAergic-anesthetics (version 1.0.0). PhysioNet. https://doi.org/10.13026/7ygq-3f91. Deposited 27 June 2023.